Forschungsstiftung Mobilkommunikation
Swiss Research Foundation on Mobile Communication
www.mobile-research.ethz.ch

Final Report
Project A2003-15
Reference 16

Final Report

Project reference: 16 (A2003-15)
Applicant's name: PD Dr. Martin Wolf
Project title: EMF and Brain: Effects on Cerebral Blood Flow, Cerebral Blood Volume and Neural Activity

1. State of Research.
1.1 Research activities performed, milestones and deliverables accomplished

Milestones	Description	Status
End of 1st month	- Exposure system installed (WP 1) - Dosimetry study (WP 2)	accomplished accomplished
End of 6th month	- Pilot study to understand nature of immediate effects: experiments and data analysis carried out (WP 3) - Protocols finalized (WP 4)	accomplished accomplished
End of 12th month	- Assessment of long-term effects: experiments carried out (WP 5) - Assessment of immediate effects: experiments carried out (WP 6) - Assessment of dose-effect relation: experiments carried out (WP 7) - Data analysis for WP 5 to 7 in progress (WP 9)	accomplished accomplished accomplished accomplished
End of 18th month	- Investigate feasibility to measure the effects of EMF on the fast neuronal signal (WP 8) - Data analysis finished (WP 9) - Composition of report and scientific publications finished (WP 10)	accomplished accomplished accomplished

Table 1: The status of the research according to the proposal

WP	Month	1	2	3	4	5	6	7	8	9	10	11	12	13	14	15	16	17	18	19	20	21	22	23
1	Exposure system set-up																							
1	Exposure system set-up																							
2	Dosimetry study																							
2	Dosimetry study																							
3	Pilot study																							
3	Measurements																							
3	Data analysis																							
4	Finalize protocols																							
4	Finalize protocols																							
5	Long-term effects																							
5	Long-term effects																							
6	Immediate effects																							
6	Immediate effects																							
7	Dose-effect relation																							
7	Dose-effect relation																							
8	Feasibility neuronal signal																							
8	Feasibility neuronal signal																							
9	Data analysis																							
9	Data analysis																							
10	Report																							
10	Report																							

Table 2: Progress of the different work packages: The main delay occurred during the set-up of the exposure system (blue = plan according to application, red = time used in reality).

1.2 Findings

1. Borderline significant immediate responses of O_2Hb and HHb to EMF were found, i.e. within 20s during exposure. These responses correspond to a decrease of CBF and CBV. They were much smaller than normal physiological changes in O2Hb and HHb elicited e.g. by functional activation of the brain. There is a relatively high probability that these responses are due to chance. Therefore these effects require further studies.
2. There was no detectable response of O_2Hb or/and HHb to EMF within 40s after exposure. The detection limit was a fraction of the normal physiological changes elicited by functional activation.
3. There was no detectable slow response of O_2Hb or/and HHb to EMF, which occurs within 20min.
4. There was no detectable dose-response relation.

Compared to previous studies using PET, NIRS provided a much higher time resolution, which allowed investigating the existence of immediate effects efficiently, non-invasively, without the use of radioactive tracers and with high sensitivity. Details are described in the draft publication.

1.3 Problems

The installation of the exposure system was not completed until June 2004 (plan January 2004). The reason for the delay of 5 months was the additional programming required to allow a free choice of intermittency periods. Since measurements cannot be carried out without the exposure system, the rest of the project was delayed as well.

The effect was smaller than expected from the preliminary data. Thus more measurements need to be carried out to secure an effect. This interfered with the aim of WP3 to explore different aspects of the nature of the effects of EMF on brain circulation. The original plan - once the most effective exposure and non-exposure periods were found - was to investigate dose-effect relations and to analyze the effect of the modulation. The prerequisite for this plan was a reproducible effect, which requires a higher number of subjects than originally expected.

In addition a smaller effect requires a more sophisticated data analysis and special filtering. This lead to a small delay in WP3.

Originally it was planned to measure long-term effects up to a duration of 30min. According to advice from the advisory committee, the subjects were asked to count backwards during the measurement to bring the brain into a defined state. This requires great discipline from the subjects and makes exceedingly long measurements difficult. The long-term effect was therefore only studied for a duration of 20min instead of 30min.

Date and Signature

Zurich, 23rd of December 2005

EMF and Brain: Effects on Cerebral Blood Flow, Cerebral Blood Volume and Neural Activity

Final progress report

PD Dr. Martin Wolf, Ph. D. Engineering, Biomedical Optics Research Laboratory,
Clinic of Neonatology, University Hospital Zurich, Frauenklinikstr. 10, 8091 Zurich

Advisory committee

As proposed by the foundation an advisory committee was created. The members are Dr. Mirjana Moser (Bundesamt für Gesundheit) and PD Dr. Peter Acherman (Institute of Pharmacology and Toxicology, University of Zurich). The members convened with Dr. Jürg Fröhlich and Prof. Niels Kuster (IT'IS) and Dr. Derek Brown and PD Dr. Martin Wolf (BORL) for the first time in February 2004 to outline of the research plan.

It was decided to investigate the following aspects of the effects of EMF on the brain during the first phase of the research (in the order of the priority):

1. Intermittency. How is the effect of EMF on the brain influenced by the intervals of exposure and non-exposure?
2. Dose-response. How do the effects vary with the dose?
3. Modulation. How do the effects depend on the modulation signal?

A second meeting of the advisory committee took place in two sessions, one with PD Dr. Peter Acherman, Prof. Niels Kuster, Dr. Jürgen Schuderer, Dr. Derek Brown and PD Dr. Martin Wolf on January 24th 2005 and one with Dr. Mirjana Moser, Dr. Jürg Fröhlich and PD Dr. Martin Wolf on February 8th 2005. Here the committee was informed about the results of the pilot study and the protocol of the main study was finalized (see below). The advisory committee also advised to prolong the study and to obtain additional funding.

Progress

WP 1: Installation of the setup of the exposure system (IT'IS)
The installation of the exposure system was not completed until June 2004 (plan January 2004). The reason for the delay of 5 months was the additional programming required to allow a free choice of intermittency periods. Since measurements cannot be carried out without the exposure system, the rest of the project was delayed as well.

WP 2: Dosimetry study (IT'IS).
The dosimetry study was carried out, however the report was not finished by IT'IS yet. It will be delivered after the closing of this report.

WP 3: Pilot study to understand the nature of immediate effects (BORL)
For WP 3 according to the suggestion of the advisory committee, the initial studies were carried out to investigate the effect of the intermittency. Thus we conducted measurements with the following protocols:

*   20s on, 40s off, N= 8
*   20s on, 60s off, N= 18
*   20s on, 120s off, N= 8
*   Sham, N= 8
*   Functional activation during motor stimulation (finger tapping), N=8

According to the decision of the advisory committee, the power of the exposure was 12W/kg peak power, i.e. 12 times higher than during the preliminary study.

It turned out that the effect was smaller than expected from the preliminary data. Thus to investigate the effect we needed a higher number of subjects during this phase and a more sophisticated data analysis (See also WP 9). Effects found during the 20s exposure / 60s non-exposure paradigm looked like an immediate response, i.e an increase of the blood circulation to EMF. For shorter or longer non-exposure periods no effect was visible. No habituation effect was found.

The lack of statistical power required an increased number of subjects.

Long-term effects were analyzed. They showed an increase in oxyhemoglobin concentration during sham and exposure, the increase being non-significantly ($p=0.14$) smaller in the exposure group than in the sham group The same was true for a decrease in the deoxyhemoglobin concentration. Again a lack of statistical power requires an increase of the number of subjects.

The original plan - once the most effective exposure and non-exposure periods were found - was to investigate dose-effect relations and to analyze the effect of the modulation. The prerequisite for this plan was a reproducible effect, which requires a higher number of subjects than originally expected.

WP 4: Development of protocol to study immediate effects, long-term effects and dose-effect relation.(BORL)

Therefore, in a second advisory committee meeting the plans were changed and it was decided to conclude WP3 without carrying out the investigation of the dose effect relation and the effect of the modulation. It was decided to focus on the most important aspects and carry out the investigation with a sufficient number of subjects.

The decision was to carry out a three armed study with $\geq$ 16 subjects. In each subject a three types of exposure (sham, 1.2W/kg and 12W/kg) were carried out. The exposure / non-exposure cycle was 20s / 60s. Thus the aims of WP 5, 6, and 7 were addressed simultaneously. Due to the delays mentioned in WP1 and WP3, the start of WP 5, 6 and 7 was delayed.

WP 5: Assessment of long-term effects

The measurements were carried out according to the protocol in 18 subjects. Two of the subjects were not used in the final analysis, because there were too many movement artifacts.

The finalized protocol provided a period of 20min for the observation of the long-term effects, because this is the maximum period subjects can remain concentrated and still enough.

The results showed no significant difference between the different conditions (sham 1.2W/kg and 12W/kg)

WP 6: Assessment of immediate effects

Protocol was carried out as described in WP4. Also no relevant immediate effects were found.

WP 7: Assessment of dose-effect relation

Protocol was carried out as described in WP4, i.e measurements at 2 exposure levels (1.2W/kg and 12W/kg). No relevant significant effects were found.

The results are described in detail in the draft publication.

WP 8: Investigate feasibility to measure the effects of EMF on the fast neuronal signal

For this purpose an ISS OxyPlex TS prototype instrument was used. The sensor of this instrument contains only optical and no electronic components and is thus inert to EMF. The light is guided to the sensor and back by silica glass fibers of 225cm length.

	AC 1	AC 2	AC 3	AC 4	DC 1	DC 2	DC 3	DC 4	PH 2	PH 3	PH 4
Difference (%)	0.0020	-0.0193	-0.0164	-0.0142	-0.0152	-0.0285	-0.0212	-0.0238	-0.0073	-0.0032	-0.0040
p (t-test)	0.7876	0.0008	0.0222	0.1289	3.9E-08	1.2E-43	9.6E-16	1.7E-15	0.0072	0.2991	0.2341

Table 1: Interferences found with a set-up with glass fibers. The frequency-domain NIRS instrument measures the mean light intensity (DC), its amplitude (AC) and phase (PH). The results of four channels are displayed. For each type of measurement significant differences were found between exposure and non-exposure periods. The size of the intereference is, however, small.

As expected the interference is much lower for this fiber optic set-up compared to our previous set-up. The results show, that the interference depends on the placement of antenna and the main instrument. When the instrument was placed behind the antenna, we encountered the least interference. Table 1 diplays the resulting difference between exposure and non-exposure periods.

The interferences found can be set in relation to optical changes resulting from changes in hemodynamics and or neuronal activation. A change in intensity of 1% for our sensor set-up leads to a change in O_2Hb or HHb of approximately 0.15µM. Thus a change in intensity of 0.03% would lead to a change in O_2Hb or HHb of approximately 0.005µM, which is negligible.

The amplitude of optical changes associated with neuronal activity is approximately 0.005% in intensity. Thus the changes due to interference are still several times higher and therefore not negligible.

To further reduce interference, in principle it is also possible to use longer fibers (10m long fibers are available for ~$12'000) and place the instrument in a different room of the exposure set-up.

Compared to the MCP II instrument, this current ISS instrument has no imaging capability. This would be a disadvantage.

WP 9: Data analysis

Evaluation of the data in WP 5 to 8: The evaluation of the signals required a much more sophisticated signal analysis than expected. We therefore employed an expert (Dr. Geert Morren) in biomedical signal analysis for 1.5 months of this project. Since the signals in the data generated in WP3 & 4 were much smaller than expected, the effort to remove noise and the filtering required more attention.

A similar data analysis was carried out for the main study.

WP 10: Composition of report and scientific publications

The final report and a publication were written.

Prof. Dr. Niels Kuster

Director Foundation IT'IS
Professor of Swiss Federal Institute of Technology – ETHZ
Phone +41 1 245 9690 · kuster@itis.ethz.ch

IT'IS FOUNDATION

Foundation for Research on Information Technologies in Society

Final Technical and Dosimetric Report

Exposure Setup for the EMF and Brain Study: Effects on CBF, CBV and Neural Activities

Sven Ebert, Jürgen Schuderer, Albert Romann, Jürg Fröhlich and Niels Kuster

Zurich, February 2006

Executive Summary

This technical report describes the human exposure setup developed and employed in the study "EMF and Brain: Effects on Cerebral Blood Flow, Cerebral Blood Volume and Neural Activity" at the Biomedical Optics Research Laboratory of the University of Zurich. The setup allows unilateral exposure of one head hemisphere with a user-defined exposure signal and strength. The exposure system has been fully characterized with complete dosimetry and uncertainty assessment. The dose for various head tissues was obtained using simulations of MRI-based phantoms. In order to evaluate the accurate dose of absorbed power within regions of the brain where the CBF and CBV are measured, additional dosimetric evaluations were performed to assess the effect of the NIRS sensor on the absorption. In addition, possible artifacts were carefully evaluated and special software was developed to enable exposure synchronized with the NIRS evaluation, thus avoiding distortions through electromagnetic interference. The setup operated during the entire exposure phase without major problems; well-defined and well-characterized exposure was achieved during all phases of exposure.

Contents

1 Introduction

Near-infrared spectrophotometry (NIRS) is highly sensitive to changes in regional cerebral blood flow (CBF) and volume (CBV) and is able to measure changes in the order of per mill. The objective of this study was to examine immediate and long-term changes in the CBF and CBV of subjects exposed to pulsed high-frequency electromagnetic fields (EMF) in a controlled cross-over study design (blinded for the subjects). The exposure setup to be developed by the IT'IS Foundation should enable the following:

- Well-defined unilateral exposure of the cortex while the NIRS sensors are mounted at the subject heads

- Minimal and well-investigated electromagnetic interference (EMI) of the exposure with the NIRS system

- Study of the influence of different amplitude modulation (AM) signals

- Investigation of dose-effect relation using different exposure levels

This technical report describes the human exposure setup developed and provides the dosimetric parameters and uncertainty assessment of the RF exposure.

2 RF Exposure Setup

The radio frequency (RF) exposure system exposes the human head unilaterally with a flexibly modulated electromagnetic field (EMF), while enabling the simultaneous measurement of CBF and CBV by means of NIRS. This allows the study of immediate and long-term changes using a blinded (for the subject) exposure design.

2.1 Setup Design

A fully computer-controlled signal unit was realized and is shown in Figure 1. It is based on an RF signal generator (Rohde & Schwarz, SML02), an arbitrary function generator (Agilent, 33120A), a 200 W power amplifier (LS Elektronik, Sweden), a bidirectional coupler with diode probes and a data logger (Agilent, 34970A). A GPIB interface is used for communication between the personal computer (PC) and the devices. The setup is depicted in Figure 2.

2.2 Modulation

Modulation is applied via two pathways:

1. The high-frequency carrier provided by the RF generator is amplitude modulated with a low frequency signal from an arbitrary function generator. The pulse structure of the GSM cocktail signal is stored on the function generator.

2. Control of the output power of the RF generator is used to adjust the power delivered to the antenna and to realize arbitrary field on/off intermittency.

The measured field values are used for feedback regulation of the output power of the RF generator. In this way, amplifier drift and impedance variations are compensated. The data logger is used for collection of the sensor signals and for generation of digital synchronization signals indicating the on/off phase of the intermittent signals.
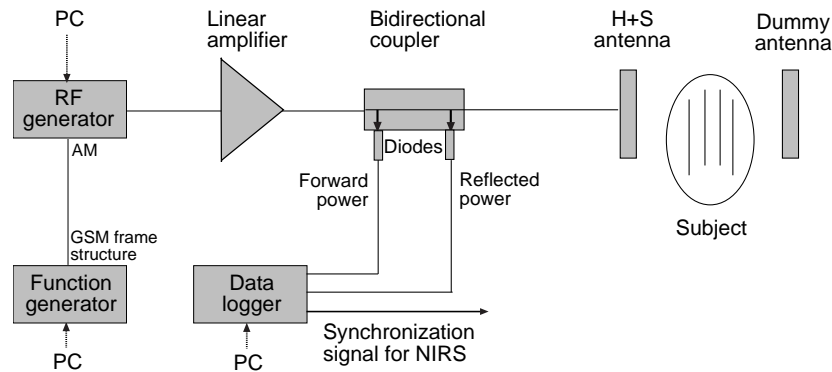
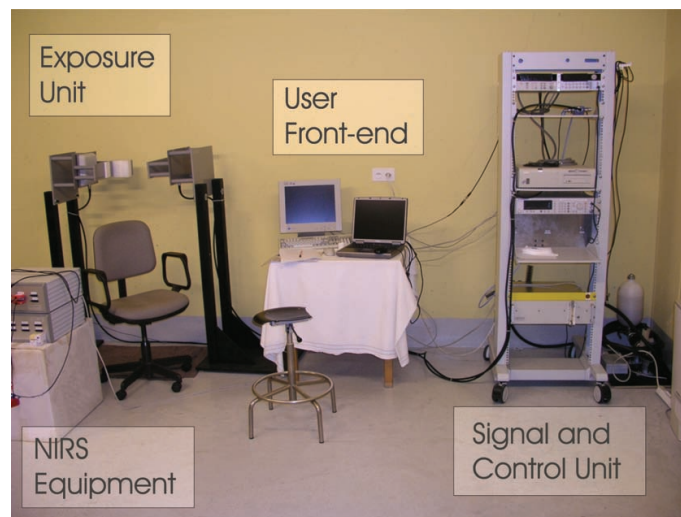Figure 1: Block diagram of the RF exposure setup.

Figure 2: RF exposure setup for NIRS at University Hospital Zurich.

Quality control of the experiments is ensured by monitoring the exposure, self-detection of malfunctions and blinded protocols:

- Monitoring: The data logger continuously records the sensor signals for forward and reflected power with a sampling rate of 0.1 Hz. All experimental parameters (settings, software commands, sensor signals) are stored in an encoded data file on the PC.

- Self-detection: The controlling and monitoring software is able to self-detect malfunctions and responds with warnings or abortions if required. Overexposure of subjects is excluded by (1) software abortion and (2) operating the amplifier close to its maximum output power and subsequent adjustment of the antenna input power using attenuators (not shown in Figure 1).

- Blind protocols: Blind study design is realized by autonomous exposure control via the PC. The software enables double-blind exposure protocols. However, in order to have better control and be able to operate various exposure schemes, it was decided that the exposure conditions should be known to the operators, but not to the test persons.

2.3   Antenna Positioning for Head Exposure

The objectives of the exposure setup were: (1) unilateral exposure, (2) exposure that mimics the exposure of a handset, as well as (3) minimal variability of the exposure from subject to subject. This was achieved using two planar, rectangular patch antennas (Huber + Suhner, SPA920/65/9/0/V) mounted on both sides of the head (Figure 3).
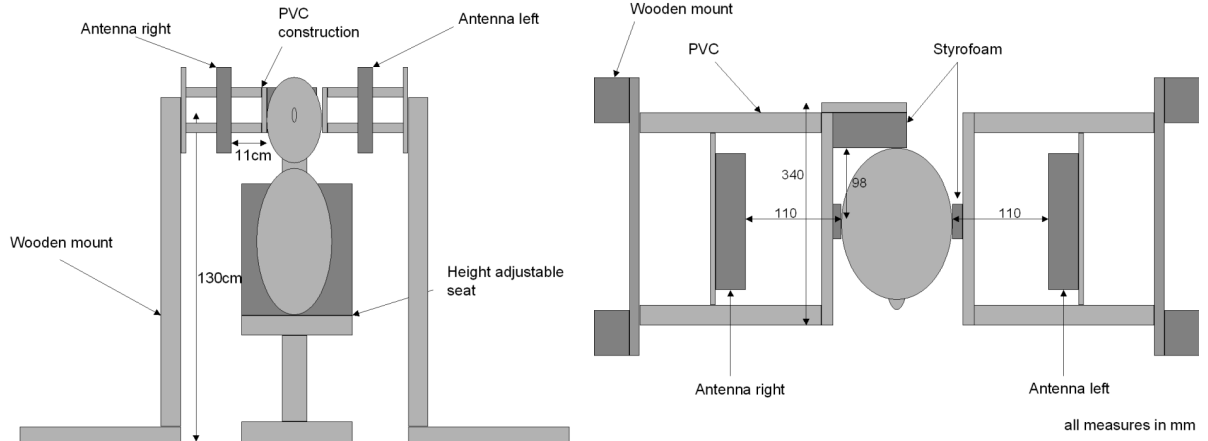

Figure 3: Mechanical sketch of the RF exposure setup.

The position was optimized with respect to achieving SAR uniformity of the exposed hemi-sphere and producing a high average SAR ratio between the exposed and non-exposed sides of the brain. The best compromise was found at 115 ± 5 mm distance between antenna and head, with the center of the antenna at 42 ± 10 mm vertically above the ear canal, i.e., approximately one third of the distance between the ear canal and the top of the head. The average SAR value of the exposed side of the head was eight times higher than that of the unexposed side.

2.4   Exposure Signals

The exposure system enables application of a wide variety of signals and exposure strengths. The operator can define the modulated signal and intermittence of exposure sequence, as well as select peak spatial-average SAR values averaged over 10 g. An on/off synchronization signal was provided to enable evaluations only during the off-phases (Figure 1).

Currently implemented exposure signals are:

- Continuous wave (CW) at 900 MHz

- Non-DTX GSM (basic) exposure simulation (upper Figure 4)

- DTX GSM exposure simulation (lower Figure 4)

- "base-station-like": This synthesized signal simulates the modulation characteristics from a GSM base station and was proposed for bioexperiments by Schüller et al. [1] (upper Figure 5). Seven (slots 0–6) of the eight bursts (duration: 0.577 ms; intermittency between bursts: 20 ms) of the basic frame (4.6 ms) were on and one off (slot 7). Frames 26, 52, 78, and 104 of the multiframe (104 basic frames) were modified: in addition to the 7th burst, the 1st burst was also idle for frames 26, 52, 78, and the 1st, 4th, and 7th bursts were idle

for frame 104. This signal structure results in the spectral components of 2, 8, and 217 Hz, and corresponding harmonics. The burst and the intermittency between the bursts led to additional components at 1.733 kHz and 50 kHz.

- "handset-like": This synthesized signal was applied by Huber et al. [2] (lower Figure 5) and designed to simultaneously simulate the ELF modulation components of the non-DTX and DTX modes of the GSM handsets .
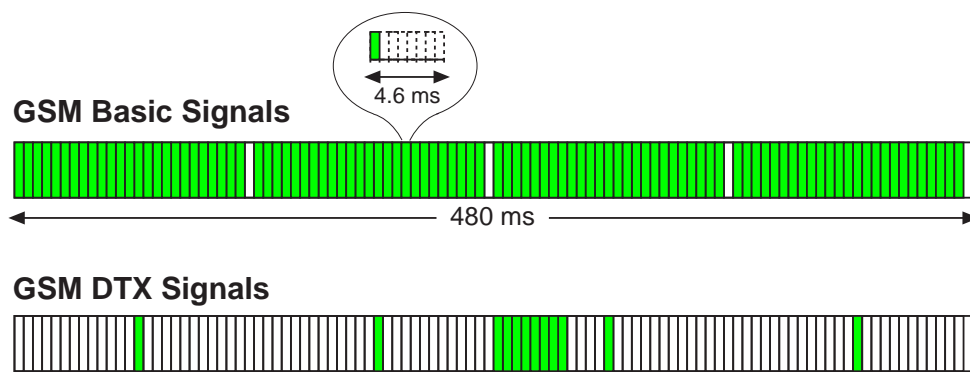
- arbitrary AM waveform of 16,000 points on request (carrier 900 MHz)

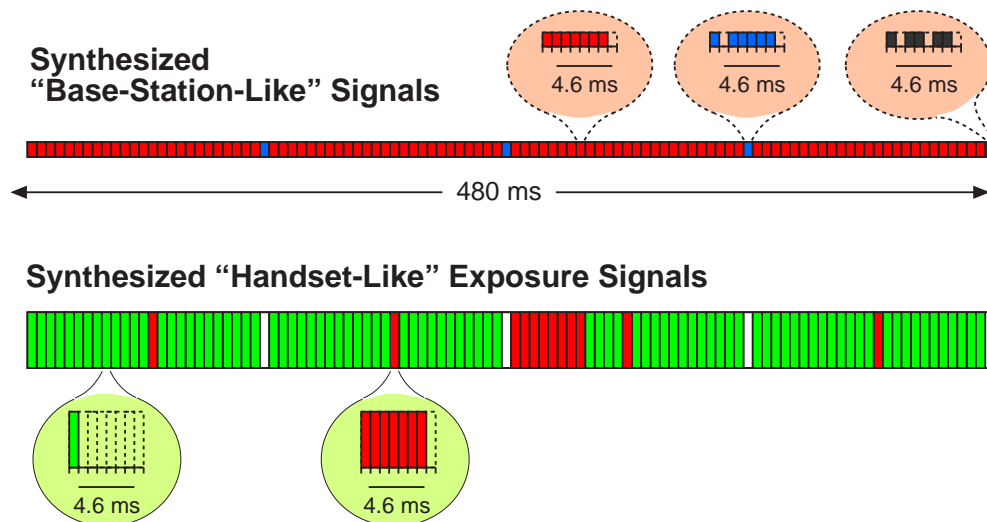Figure 4: Pulse structure of GSM signals (GSM basic and DTX modes) with a multi-frame period of 480 ms.

Figure 5: Synthesized GSM signals simulating the ELF components of base stations and handsets (non-DTX and DTX).

The dynamic range for time-averaged peak spatial-average SAR averaged over 10 g was from 0 to 50 W/kg (peak slot average). This enabled application of 0, 0.6 and 6 W/kg peak spatial-average SAR for the handset-like exposure signal. The evaluation sequence was 2 s on and 2 s off while the intermittence was 20 s on and 40 s off for 15 cycles. The peak spatial-average SAR time-averaged over the entire exposure duration was therefore 0, 0.1 and 1 W/kg.

3 Dosimetry

The following approach was taken to obtain reliable dosimetric data with acceptable effort. In the first step the analysis was conducted without any sensor attached, and in the second step the effect and distortion by the sensors was determined. This approach is suitable since the distortion is local and less dependent on individual anatomy exposure from the setup, i.e., the uncertainties can be evaluated independently.

The detailed dosimetry is based on simulations and provides SAR estimations for functional subregions inside the brain. A series of measurements in free space and inside dielectric head phantoms were performed for verification purposes: (1) verification of the modeling of the antennas including the feeding source by measurements of the incident fields, and (2) verification of the simulated induced fields inside homogeneous phantoms. In addition, measurements were conducted to assess the effect of the electrodes on the induced fields (shielding/reflection and induced contact currents). The computational tool SEMCAD (Schmid & Partner Engineering AG, Zurich, Switzerland; www.semcad.com) was employed as the simulation platform in this study. SEMCAD is based on the finite difference time domain (FDTD) method and is enhanced with unique features for RF dosimetry, such as highly nestable subgrids and a special compound format enabling the handling of non-homogeneous human models. The code has been broadly validated (e.g., [3] and [4]). The setup dosimetry is based on the human head model derived from the dataset of the head of a healthy female subject (age 40 years), consisting of 121 magnetic resonance imaging (MRI) slices, with a slice separation of 1 mm in the ear region and 3 mm for the rest of the head [5]. Figure 6 shows the SAR distributions in the axial, coronal and sagittal cross-sections of the head. The SAR distribution on the surface of the head (skin) is depicted in Figure 7.
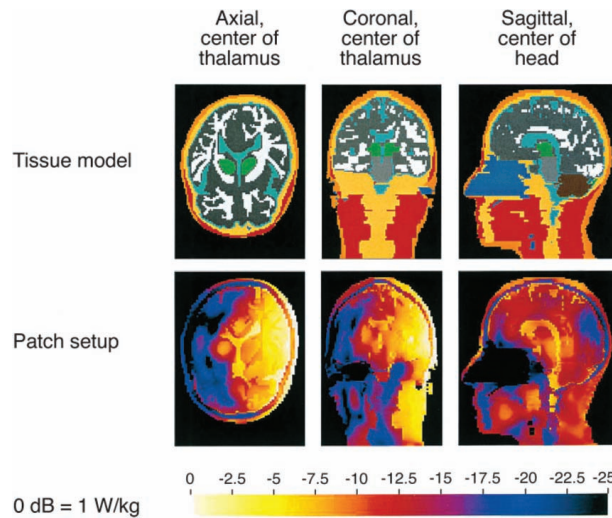

Figure 6: Axial, coronal and sagittal SAR distributions in the exposed head.
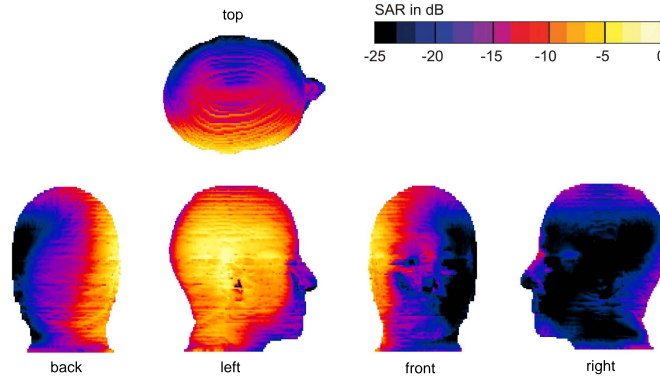
Figure 7: Normalized surface SAR distribution.

The precision of the discretization of the brain has been improved, and functional subregions have been derived from the original MRI slices. Table 1 shows the dielectric parameters of the 23 discriminated tissues, set according to the values given in Gabriel [6]. For the quantification of left/right asymmetries of the SAR distribution in the head, the phantom was divided into two evaluation volumes. In order to enable maximum spatial resolution in the area of interest, an optimized graded mesh was used with a minimum voxel size of $1\,\text{mm}^3$ in the exposed head region (total number of voxels approx. 15 million). The postprocessor of SEMCAD provided statistical data for each tissue type as well as for defined head areas (left side, right side, and entire head), e.g., mean SAR along with standard deviation (SD) and 1 g averaged peak spatial-average SAR were computed.

The antenna units were modeled with voltage sources and harmonically excited at 900 MHz until a steady state was reached. The patch antenna was excited via a microstrip feedline, whereby the voltage source was located between the feedline and the metallic N-type plug holder. For field measurements, the near field scanner DASY4 (Schmid & Partner Engineering AG, Zurich, Switzerland) was employed, equipped with the latest generation of free space and dosimetric probes (Table 2). DASY4 is based on a precisely controlled, 3-axis robotic arm which can position all sorts of dosimetric probes. It allows highly sensitive field and temperature measurements in free space and inside phantoms. Verification of the appropriate modeling of the RF sources was conducted with the generic twin phantom [7] filled with a homogeneous tissue simulating liquid.

3.1 Peak Spatial-Average SAR and SAR Distributions

The model of the patch antenna has been validated based on experimental far- and near-field data [3]. Due to the close proximity to the head, the patch setup has a high efficiency of about $0.54\,\text{W/kg}$ per Watt antenna input power. Higher efficiency provides the advantage of enabling the application of signals with high crest factors, such as GSM basic (crest factor of 8.3) and DTX (crest factor of 69.3) with reasonable peak power requirements (crest factor pulse peak power/average power). The results of the numerical analysis are shown in Table 2 and confirm that a strong asymmetrical exposure has been achieved (rightmost column of Table 2). The position of the head with respect to the EM source can be kept very constant (variations of position $< \pm 5\,\text{mm}$ horizontally and $< \pm 30\,\text{mm}$ in the plane of the patch antenna). The variations and uncertainties (Table 4) were assessed according to the methodology in [2].

Tissue type	ϵ_r	σ [S/m]
Blood	61.4	1.54
Bone (cancellous)	20.8	0.34
Brain (grey matter)	52.7	0.94
Brain (white matter)	38.9	0.59
Cerebellum	49.4	1.26
Cerebro-spinal fluid	68.6	2.41
Cornea	55.2	1.39
Ear (average skin and cartilage)	42.0	0.82
Fat	5.5	0.05
Glands	59.7	1.04
Lense	46.6	0.79
Lower jaw	20.8	0.34
Middle brain (grey matter)	52.7	0.94
Muscle	55.0	0.94
Skin	41.4	0.87
Skull	20.8	0.34
Spinal cord (grey matter)	52.7	0.94
Spine	82.5	0.57
Thalamus (grey matter)	52.7	0.94
Tongue	55.3	0.94
Upper jaw	20.8	0.34
Lateral ventricles	68.6	2.41
Vitreous humor	68.9	1.64
Generic phantom liquid	41.5	0.97

Table 1: Tissue types discriminated in the human head model with dielectric parameters for 900 MHz (relative permittivity ϵ_r and conductivity σ according to [6]).

SPEAG probe type	Probe diameter [mm]	Dynamic range	Deviation of axial isotropy [dB]	Deviation of spherical isotropy [dB]
ET3DV6	6.8	0.002–100 W/kg	$< \pm 0.05$	$< \pm 0.20$
EF3DV2	3.9	2–1000 V/m	$< \pm 0.05$	$< \pm 0.30$
H3DV3	5.0	0.01–2 A/m	$< \pm 0.05$	$< \pm 0.20$

Table 2: Characteristics of the free space and dosimetric SPEAG probes used for field mapping.

Tissue	Right hemisphere $psSAR_{1g}$	$psSAR_{10g}$	SD	Left hemisphere $psSAR_{1g}$	$psSAR_{10g}$	SD	$Ratio_{10g}$
Grey matter	1.02	0.25	0.19	0.15	0.03	0.03	8.3
White matter	0.61	0.20	0.13	0.08	0.02	0.01	10
Grey and white matter	0.97	0.24	0.18	0.14	0.03	0.02	8
Thalamus	0.16	0.13	0.02	0.13	0.10	0.03	1.3
Brain avg.	1.55	0.27	0.26	0.33	0.04	0.05	6.7
Brain avg. (without lateral ventricle)	0.97	0.24	0.18	0.15	0.03	0.03	8

Table 3: Head tissue specific peak spatial-average SAR averaged over 1 g ($psSAR_{1g}$) and 10 g ($psSAR_{10g}$) with standard deviation (SD) and ratio between left and right hemispheres. The brain-averaged values include grey matter, white matter, cerebellum, middle brain, thalamus, cerebro-spinal fluid (CSF) and lateral ventricles.

Tissue	Variation (k = 1) [%]	Uncertainty (k = 1) [%]
Grey matter	20	16
White matter	18	16
Grey and white matter	20	16
Thalamus	29	16
Brain av. (incl. vent.)	18	16
Brain av. (without vent.)	18	16

Table 4: Estimated exposure variations and uncertainties.

3.2   Validation of the Simulation Model

The numerical dosimetry was verified by replacing the non-homogenous phantom with the generic twin phantom filled with tissue simulating liquid ($\epsilon_r = 41.2$ and $\sigma = 0.85\,\text{S/m}$). This setup was experimentally and numerically analyzed, and areas as well as peak spatial-average SAR values were compared. The deviation between measurement and simulation of less than 10% for the $1\,\text{g}$ and $10\,\text{g}$ averaged peak spatial-average SAR confirmed the high quality of the numerical models.

3.3   SAR Distortion by NIRS Sensors

The NIRS sensors are rather large and will effect the SAR distributions as well as their connecting cables. Therefore the effect had to be carefully analyzed and standardized configurations defined. The evaluation was conducted using the SAM head phantom with the DASY4 system (SPEAG, Switzerland). Influence of the sensor on the SAR distribution has been determined as described in the following. The phantom head was filled with tissue simulating liquid ($\epsilon_r = 41$ and $\sigma = 0.95$). The antenna was positioned at $100 \pm 2\,\text{mm}$ distance from the ear with its center $42 \pm 2\,\text{mm}$ above the ear reference point during the experiments. Two sensor positions were evaluated on the left head section of the SAM phantom:

- Sensor above ear: The NIRS sensor was positioned just above the ear of the SAM phantom. Two different configurations were analyzed: (1) sensor cable parallel to the polarization of the E-field as emitted from the antenna (worst-case configuration for RF coupling) and (2) sensor cable perpendicular (best-case for low RF coupling). In both positions, the sensor surface is parallel to the orientation of the patch antenna.

- Sensor at motor cortex: The NIRS sensor was positioned at the location of the motor cortex with the sensor cable perpendicular to the polarization of the E-field (study configuration). Here the sensor surface is perpendicular to the orientation of the patch antenna.

The tested configurations were:

1. Reference configuration, no sensor (REF): SAM phantom with patch antenna located below the left head section. The distance between the head and the antenna corresponds to the exposure system applied for the study.

2. Sensor at SAR maximum, cable parallel (Max, parallel): Reference configuration including the NIRS sensor positioned at the location of the maximum SAR measured for the reference configuration. The cable connecting the sensor to the hardware unit is oriented parallel to the incident E-field.

3. Sensor at SAR maximum, cable perpendicular (Max, perpendicular): Reference configuration including the NIRS sensor positioned at the location of the maximum SAR measured for the reference configuration. The cable connecting the sensor to the hardware unit is oriented perpendicular to the incident E-field.

4. Sensor shifted, cable parallel (Shifted, parallel): Reference configuration including the NIRS sensor positioned at the outermost measurement point of the area scan allowing an entire zoom scan. The cable connecting the sensor to the hardware unit is oriented parallel to the incident E-field.

5. Sensor shifted, cable perpendicular (Shifted, perpendicular): Reference configuration including the NIRS sensor positioned at the outermost measurement point of the area scan allowing an entire zoom scan. The cable connecting the sensor to the hardware unit is oriented perpendicular to the incident E-field.

6. Study configuration, perpendicular (Study): Reference configuration including the NIRS sensor positioned at the corresponding location of the motor cortex on the human head. The cable connecting the sensor to the hardware unit is oriented perpendicular to the incident E-field.

Depending on the location of the NIRS sensor, different zoom scans were carried out, identified as follows:

- Scan 1 (SAR max$_{REF}$): Zoom scan centered at the measured maximum SAR of the area scan of the reference configuration.

- Scan 2 (cortex): Zoom scan centered below the NIRS sensor at the outermost point of the area scan at which zoom scan evaluation is possible within the valid phantom region (close to the area of the motor cortex).

- Scan 3 (SAR max$_{NIRS}$): Zoom scan centered at the location of the measured maximum of the SAR of the area scan with the attached NIRS sensor (sensor position depends on configuration).

In Table 5 the maximum peak spatial-average SAR values and their deviations from the reference are summarized for the evaluated configurations. Figures 8 to 13 show the corresponding SAR distributions. The influence of the NIRS sensor can be clearly identified. As expected, the orientation of the cable has a large influence on the SAR distribution. The influence on the SAR distribution decreases the further the sensor is positioned above the ear. The two uppermost Figures 8 and 9 compare the reference configuration without sensor to the study configuration with sensor at the motor cortex. Only low field distortions are observed.

There can be considerable deviation in the maximum of the peak spatial-average SAR for 10 g and 1 g. Therefore it is necessary to pay attention to the orientation of the cable with respect to the incident E-field. This can also be seen in the corresponding area scans (Figures 8 to 13). If this is taken into account, the deviations compared to the reference situation are below $\pm$ 0.4 dB. The sensor causes slightly higher maximum peak spatial-average SAR values in the head. However, for the doses used in the study the values are still much below those required by current safety guidelines.
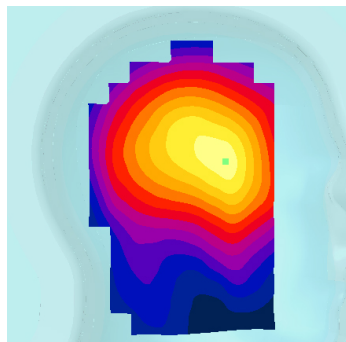
local SAR relative to peak spatial SAR of 10g
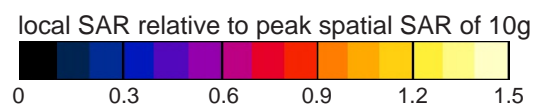
0   0.3   0.6   0.9   1.2   1.5

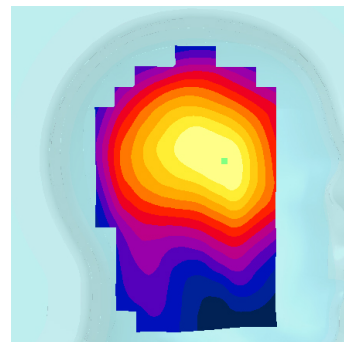Figure 8: SAR distribution for the reference configuration.

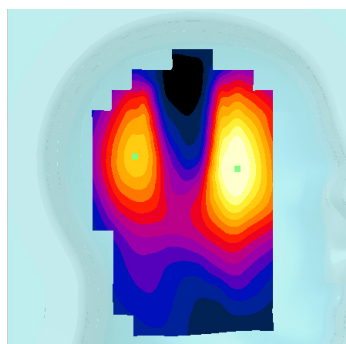Figure 9: SAR distribution for configuration 6.

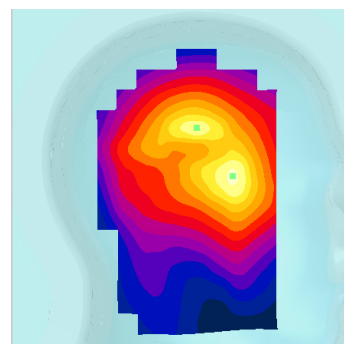Figure 10: SAR distribution for configuration 2.
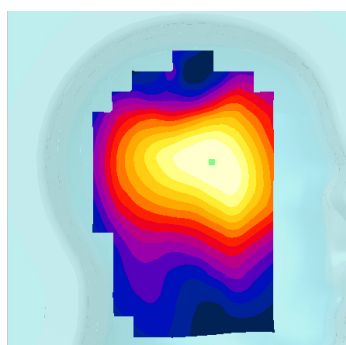
Figure 11: SAR distribution for configuration 3.
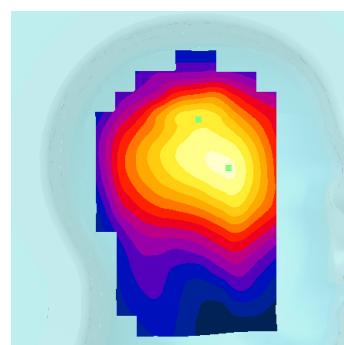
Figure 12: SAR distribution for configuration 4.

Figure 13: SAR distribution for configuration 5.

Configuration	Scan 1 (SAR max$_{REF}$)		Scan 2 (cortex)		Scan 3 (SAR max$_{NIRS}$)	
	$psSAR_{10g}$ [dB]	$psSAR_{1g}$ [dB]	$psSAR_{10g}$ [dB]	$psSAR_{1g}$ [dB]	$psSAR_{10g}$ [dB]	$psSAR_{1g}$ [dB]
2 (Max, parallel)	-0.8	0.3	-	-	0.4	0.6
3 (Max, perpend.)	0.3	-0.2	-	-	0.1	0.4
4 (Shifted, parallel)	-	-	-3.0	-2.3	-	-
5 (Shifted, perpend.)	-	-	-0.2	0.1	0.3	0.3
6 (Study)	-	-	-	-	0.2	0.2

Table 5: Deviations of maximum peak spatial-average SAR values for 10 g ($psSAR_{10g}$) and 1 g ($psSAR_{1g}$) for the evaluated configurations from the reference configuration.

4 Electromagnetic Interference of NIRS Equipment

The effects of electromagnetic interference (EMI) to the NIRS equipment from exposure was evaluated using the same configuration as above. The antenna input power was varied within the range of 0.1 W to 40 W, corresponding to a peak spatial-average SAR averaged over 1 g from 0.06 to 26 W/kg. RF power was manually switched in a 20 s on/off scheme. Concurrently, a signal was provided to the data acquisition unit of the NIRS detector. The NIRS recording channels were analyzed separately. Average values, standard deviations and the range of interference signals were evaluated.

Table 6 summarizes the electromagnetic interference measurement data for the different tested conditions. Optical sensor signals for the light intensity at the detector are given as the AD values after the AD converter. In Figure 14 the worst-case EMI on NIRS is shown. It corresponds to: (1) NIRS sensor above ear, sensor lead parallel to incident E-field, (2) average input power 5 W (peak power of pulses: 24 W, peak spatial-average SAR (10 g) = 2.5 W/kg) and (3) source-detector pair with the highest amount of interference.

The black trace in Figure 14 approximately depicts the size of the change in the optical signal corresponding to a localized change of 6% in cerebral blood flow as found during PET studies [8]. Although the power of the EMI is 2.5 times higher than the one we will use for human subjects, the induced signal changes (blue trace) are in the order of magnitude of the expected signal. Since the interference is pulsed, it can be removed using a median filter of 0.25 s width (red trace). Additionally, it is possible to evaluate the data only during RF off phases, indicated by a synchronized signal (green trace).

With respect to electromagnetic interference, the following conclusions can be drawn:

1. The main difference between the optical signal during EMI and without EMI depends linearly on the power of the EMI irradiation. The influence of EMI disappears immediately after the RF power is switched off (or after a GSM pulse). NIRS measurements during RF off phases are therefore free of artifacts. An ideal time resolution to detect hemodynamic changes can be obtained by alternating 2 s RF on with 2 s RF off or even smaller.

2. The interference varies depending on the location of the LEDs and photodiodes within the NIRS sensor and mostly affects the detector side. In the worst case, the interference can reach the level of the expected changes in cerebral blood flow (as derived with PET).

Worst case of pulsed electromagnetic interference (EMI) on near infrared spectrophotometry (NIRS)
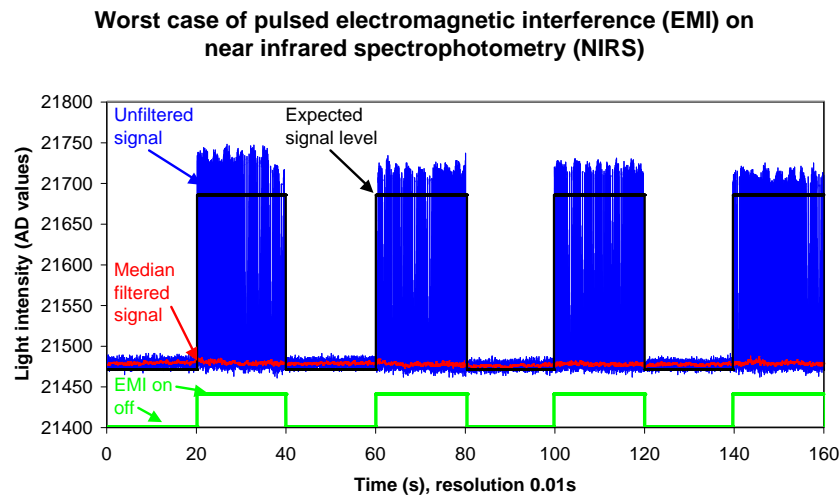
Figure 14: The influence of the pulsed electromagnetic interference (EMI) with a mean power of 5 W on the near infrared spectrophotometry (NIRS) signal (blue trace). The black trace approximately depicts the size of the change in the optical signal corresponding to a localized change of 6% in cerebral blood flow as found during PET studies. The interferences can be removed using a median filter of 0.25 s width (red trace) or by only evaluating data during the RF off phases (green trace).

Location NIRS sensor	Direction sensor cable	Modulation	Power [W]	Avg. diff. AD	SD AD
Above ear	parallel	CW	0.1	0.23	4.9
Above ear	parallel	CW	1	2.3	2.5
Above ear	parallel	CW	5	10	4.4
Above ear	parallel	CW	40	79	9.6
Above ear	parallel	AM	0.1	0.21	0.36
Above ear	parallel	AM	1	2.3	3.2
Above ear	parallel	AM	5	11	15
Above ear	perpend.	CW	40	16	117
Above ear	perpend.	AM	5	1.6	17
Motor cortex	perpend.	AM	5	2.3	4.8

Table 6: The NIRS sensor signal dependencies (average difference (AD) between optical signals with and without EMI has) have been investigated for sensor location at the SAM phantom, cable orientation relative to the incident E-field (parallel or perpendicular), signal modulation, and delivered antenna input power.

3. A median filter completely removes the artifacts caused by pulsed EMI in the optical signal. Thus, hemodynamic changes can be detected with this setup. However, applying the median filter reduces the time resolution, such that the fast neuronal signal cannot be assessed.

Based on these investigations a protocol was defined that minimizes possible artifacts due to EMI.

5 Conclusions

This technical report describes a human exposure setup which enables unilateral exposure of a head hemisphere with various user-adjustable exposure schemes and exposure strengths. The exposure system has been characterized, and a dosimetry and uncertainty assessment was performed. The doses for various head tissues were extracted from simulations. During this study, the setup has operated without major difficulties and delivered well-defined exposure.

Acknowledgments

References

[1] M. Schüller, J. Streckert, A. Bitz, K. Menzel, and B. Eicher, "Proposal for generic GSM test signal," in *Proceedings of the 22nd BEMS Annual Meeting*, 2000, pp. 122–123.

[2] R. Huber, J. Schuderer, T. Graf, K. Jütz, A. A. Borbély, N. Kuster, and P. Achermann, "Radio frequency electromagnetic field exposure in humans: Estimation of sar distribution in the brain, effects on sleep and heart rate," *Bioelectromagnetics*, vol. 24, no. 4, pp. 262–276, May 2003.

[3] A. Christ, "Analysis and improvement of the numerical properties of the FDTD algorithm," PhD thesis, Diss. ETH Nr. 15057, Eidgenoessische Technische Hochschule, Zuerich, Switzerland, 2003.

[4] N. P. Chavannes, "Local mesh refinement algorithms for enhanced modeling capabilities in the FDTD method," PhD thesis, Diss. ETH Nr. 14577, Eidgenoessische Technische Hochschule, Zuerich, Switzerland, 2002.

[5] M. Burkhardt and N. Kuster, "Appropriate modeling of the ear for compliance testing of handheld MTE with SAR safety limits at 900/1800 MHz," *IEEE Transactions on Microwave Theory and Techniques*, vol. 48, no. 11(1), pp. 1921–1934, Nov. 2000.

[6] C. Gabirel, "Compilation of the dielectric poperties of body tissues at RF and microwwave frequencies," Report N.AL/OE-TR-1996-0037, Occupational and environmental health directorate, Radiofrequency Radiation Division, Brooks Air Force Base, Texas (USA), Tech. Rep., June 1996.

[7] N. Kuster, R. Kästle, and T. Schmid, "Dosimetric evaluation of handheld mobile communications equipment with known precision," *IEICE Transactions on Communications*, vol. E80-B, no. 5, pp. 645–652, May 1997.

[8] R. Huber, V. Treyer, A. A. Borbely, J. Schuderer, J. M. Gottselig, H.-P. Landolt, E. Werth, T. Berthold, N. Kuster, A. Buck, and P. Achermann, "Electromagnetic fields, such as those from mobile phones, alter regional blood flow and sleep and waking eeg," *Journal of sleep research*, vol. 11, pp. 289–295, 2002.